

Anomalous grazing incidence small-angle x-ray scattering studies of platinum nanoparticles formed by cluster deposition

Byeongdu Lee^{a)} and Sönke Seifert

Experimental Facility Division, Argonne National Laboratory, 9700 South Cass Avenue, Argonne, Illinois 60439

Stephen J. Riley, George Tikhonov, Nancy A. Tomczyk, and Stefan Vajda

Chemistry Division, Argonne National Laboratory, 9700 South Cass Avenue, Argonne, Illinois 60439

Randall E. Winans

Experimental Facility Division, Argonne National Laboratory, 9700 South Cass Avenue, Argonne, Illinois 60439 and Chemistry Division, Argonne National Laboratory, 9700 South Cass Avenue, Argonne, Illinois 60439

(Received 23 September 2004; accepted 21 June 2005; published online 19 August 2005)

The size evolution of platinum nanoparticles formed on a SiO₂/Si(111) substrate as a function of the level of surface coverage with deposited clusters has been investigated. The anisotropic shapes of sub-nanometer-size nanoparticles are changed to isotropic on the amorphous substrate as their sizes increased. Using anomalous grazing incidence small-angle x-ray scattering (AGISAXS), the scattering from nanoparticles on the surface of a substrate is well separated from that of surface roughness and fluorescence. We show that AGISAXS is a very effective method to subtract the background and can provide unbiased information about particle sizes of less than 1 nm. © 2005 American Institute of Physics. [DOI: 10.1063/1.1999627]

I. INTRODUCTION

Metallic nanoparticles have been intensively studied for their optical, electronic, and catalytic properties (see, for example, Refs. 1–6). For example, these studies have shown that the catalytic activity and selectivity of the nanoparticles strongly depend on particle size, composition, and shape, as well as the substrate material.^{4–6} These extraordinary catalytic properties can be strongly altered and the catalytic activity can be lost due to the sintering process taking place at elevated temperatures or upon exposure to mixtures of reactive gases.⁷ Therefore, the size and shape measurements of the metallic nanoparticles in certain matrixes or on the substrates are indispensable in determining the correlation to their physical and chemical properties. Anomalous small-angle x-ray scattering (ASAXS) has been used for studying particles buried in a matrix.^{8–10} For instance, Vad *et al.* studied 1-nm-size Pt particles embedded in organic matrixes and demonstrated that the size distribution obtained by ASAXS is well matched with that determined by transmission electron microscopy (TEM).⁸ Since the atomic scattering factor of the metal near the x-ray energy of its absorption edge varies, while the atomic scattering factor of the matrix does not, it is possible to use the contrast variation method by varying the x-ray energy instead of varying the material as is normally done. When particles are deposited on the surface of the substrate, ASAXS, which is normally done in a transmission geometry, is not applicable because of the limited sampling volume. Instead, grazing incidence small-angle x-ray scattering (GISAXS) can be used in combination with

the anomalous technique. GISAXS is an emerging technique for studying the shapes, sizes, and spatial correlation of nanoparticles on the substrate,^{11–14} as well as embedded in the substrate^{15–17} or in a film on the substrate.^{18,19} GISAXS is similar to SAXS but differs in the measurement geometry. GISAXS is performed in reflection mode whereas SAXS is performed in transmission mode. Recent studies of Renaud *et al.* demonstrated the high sensitivity of the GISAXS technique to monitor the real time growth of Pd clusters on MgO(100) and of Co on Au(111) during metal-vapor deposition.¹² This work has been extended to a quantitative study of the growth of Pd particles on MgO.¹³ Lee *et al.* studied size distributions of approximately 1-nm nanopores in a 100-nm-thick film on the Si substrate using GISAXS.¹⁸ In most cases of GISAXS experiments, the incident angle of x-ray beam to the surface of bare or thin-film-coated substrate is chosen close to the critical angle of the substrate, $\alpha_{c,s}$, yielding an enhanced SAXS intensity. Reflection and refraction, which occur at a small incident angle and unavoidably distorts the scattering of particles, have been successfully taken into account by a new theoretical model developed under the distorted wave Born approximation (DWBA).^{12,14,15,19}

A problem with GISAXS is a lack of a quantitative background subtraction method. When nanoparticles are supported on or buried in the substrate, scattering from the substrate structures, such as surface roughness^{20,21} and morphological structures, are unavoidably mixed with that from particles. One exception is when the concentration of the studied particles is much higher than that of the surface structures. Up to now, scattering from substrate roughness has been estimated and subtracted from the total signal by an

^{a)} Author to whom correspondence should be addressed. Electronic mail: blee@aps.anl.gov

TABLE I. GISAXS results from best fits and Guinier analysis for Pt clusters deposited on a SiO₂/Si(111) substrate with different levels of initial surface coverage. (The level of coverage was varied by the number of vaporization laser shots applied on the platinum rod.) The parameter r_0 is the radius and its deviation σ from the cylinder model. Its height is assumed to be correlated with the radius with factor of H/R . The $R_{g,i}$ and $R_{g,o}$ represent the radius of gyrations along the directions of in plane and out of plane respectively. The interparticle distance obtained by maximum position of the structure factor is D .

S	Surface coverage Pt atoms/cm ²	Cylinder model					Sphere model		$D(\text{\AA})$
		$r_0(\text{\AA})$	σ	H/R^a	$R_{g,i}(\text{\AA})^b$	$R_{g,o}(\text{\AA})^c$	$R_{g,i}(\text{\AA})^b$	$R_{g,o}(\text{\AA})^b$	
1	1.4×10^{14}	6.3 ± 0.2	0.26 ± 0.01	1.27	7.4 ± 0.3	4.7 ± 0.2	8.9 ± 0.3	7.1 ± 0.1	20.4 ± 2
2	3.4×10^{15}	8.1 ± 0.2	0.25 ± 0.01	1.38	9.5 ± 0.2	6.6 ± 0.2	9.6 ± 0.3	6.7 ± 0.1	31 ± 3
3	6.8×10^{15}	8.0 ± 0.3	0.40 ± 0.02	1.46	19.9 ± 0.3	14.5 ± 0.2	19.4 ± 0.3	15.6 ± 0.1	
4	1.4×10^{16}	$^{d}28.3 \pm 0.3$	$^{d}27.0 \pm 0.3$	

^aHeight/radius.

^bCalculated from fitted distribution functions.

^cCalculated as $\frac{1}{2}R_{g,i} H/R$.

^dObtained from Guinier analysis.

approximation based on assumptions of asymptotic behaviors of scattering intensity as a power law whose exponent is varying depending on models of surface roughness.²⁰ This approach is only useful as a method to approximate backgrounds at the small-angle region and acceptable when the signal is obviously obeying the known power-law. In addition, since such a power-law behavior is common in the small-angle x-ray scattering (SAXS) of particles,²² it should be proven to have its origin solely in the substrate, not in the nanoparticles or a film on the substrate. The wide angle region where the power-law scattering is measured (so-called Porod region) is differentiated from the very small-angle region (so-called Guinier region) where the scattering is only dependant on the overall particle size and not the shape. For example, a scattering vector of $q=0.1 \text{ \AA}^{-1}$ represents Guinier region for a sphere with a 10- \AA radius, while the same q corresponds to a Porod region for a 100- \AA radius sphere. Power-law values in the Porod region are determined by the surface structure and the shape of the single particle.²² Power values between -3 and -4 represent the fractal surface and powers less than -4 represent the gradient surface. Powers of -2 and -4 are for the aligned and random parallel-piped surfaces, respectively.^{12,22} If the particles are aggregated into fractals and form a mass fractal, the power law can be less than -2 .²² Except for these power-law backgrounds, as the particle sizes become as small as a few Angstroms, the removal of any additional background scattering signal from the total signal is becoming exceedingly difficult. Since the scattered intensities of GISAXS are sensitive to the width and thickness of the film, surface structure of the substrate, incident angle, and amount of particles, it is difficult to calculate the corresponding weight factors for the independently measured GISAXS of the substrate and nanoparticles on the substrate to reduce the purely nanoparticle scatterings, as is generally done for the SAXS data. If the surface morphology of the substrate is not a flat crystal surface, or if its changes occur during the sample preparation, the estimation background scattering becomes even more difficult.

In this paper, we will present a new method based on anomalous GISAXS (AGISAXS) which allows differentiation of particle scattering from the other types of scattering including a substrate roughness. We report for the first time

the AGISAXS results on Pt nanoparticles produced by the deposition of clusters on a SiO₂/Si(111) substrate.

II. EXPERIMENT

The experimental setup and the design of the cluster source have been described in detail elsewhere,^{23,24} and only details concerning the cluster deposition are given here. A beam of platinum clusters was produced in a cluster source with a 1-cm channel length by vaporizing the metal from a platinum rod with a frequency-doubled yttrium aluminum garnet (YAG) laser operating at a repetition rate of 50 Hz and using helium as a carrier gas. A substrate holder, capable of holding up to six substrates, was mounted on a translation stage and positioned at a distance of 5 cm from the nozzle of the source. Using a mask placed in front of the substrate, a 5.2-mm-diameter area of the substrate was exposed to the cluster beam. In this arrangement, the full distribution of clusters produced in the source was used for deposition.²⁵ The substrate chosen was a naturally oxidized silicon wafer [SiO₂/Si(111)]. The degree of coverage of the substrate surface with clusters was controlled by varying the number of shots of the 50-Hz vaporization laser applied on the metal target rod (see Table I). Samples with surface coverage up to 1.7×10^{16} Pt atoms/cm² were prepared in order to study the effect of the level surface coverage on the size of the nanoparticles formed on the SiO₂/Si(111) substrate.

The AGISAXS experiments were performed at the BESSRC beamline 12ID-C at the Advanced Photon Source (APS) at Argonne National Laboratory using monochromatic x rays with energies near the L_3 -absorption edge of Pt ($E = 11.564$ keV). Before the scattering measurement, energies were calibrated by using the absorption edge of a standard Pt foil. Three detectors were used: an ion chamber for the measurement of incoming beam flux, a pin diode for the transmitted or reflected primary beam, and a 2048×2048 -pixel two-dimensional (2D) MarCCD detector for recording the AGISAXS images from the sample. The detector was positioned about 0.9 m from the sample. The incident angle was kept at 0.14° , close to the critical angle of the SiO₂/Si(111) substrate for total reflection. A beam stop masked the intense specularly reflected beam and the diffuse scattering along the plane of the specular x-ray beam. The 2D data were cor-

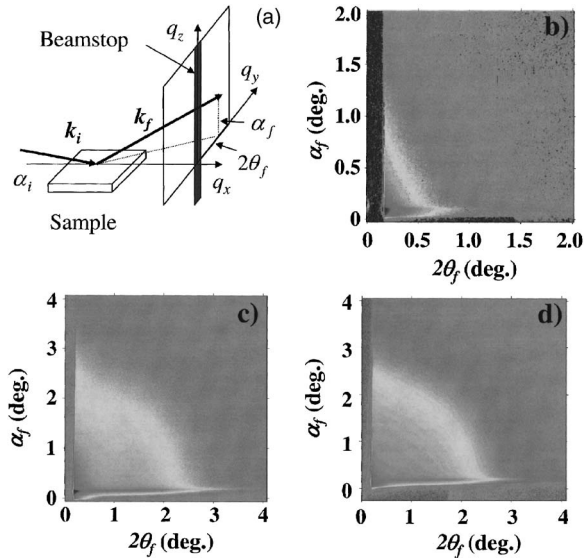


FIG. 1. Scheme of the GISAXS geometry used in the experiment (a) and the GISAXS images plotted in logarithmic scales for the $\text{SiO}_2/\text{Si}(111)$ substrate (b), sample 1 (c), and sample 2 (d).

rected for the dark current, nonuniform intensity, and pixel distortion of the charge-coupled device (CCD) detector. The camera length was calibrated using a standard (silver behenate) with known lattice spacing.

III. RESULTS AND DISCUSSION

Figure 1(a) shows the geometry of GISAXS. The incident and exit x-ray beams are characterized by wave vectors k_i and k_f defined by the in-plane and out-of-plane angles, $2\theta_f$, α_i , and α_f , respectively. Figures 1(b)–1(d) show the scattering from the bare Si wafer, samples 1 and 2, respectively. The in-plane intensity of the bare substrate in Fig. 1(b) is comparable to the particle scattering when the particle size is small and the level of surface coverage is low, as shown in Figs. 1(c) and 1(d). This scattering from the surface roughness originates from the contrast between the Si/SiO₂ and the vacuum. Thus it is strongest at the critical angle α_c of Si of about 0.14° and is elongated along the out-of-plane direction.

We measured nine AGISAXS patterns for all samples near the L_3 -absorption edge of Pt from 4 eV above to 192 eV below the edge, which makes it possible to vary the contrast for scattering of that particular element. This systematic variation in contrast yields the partial scattering functions of the specific atomic species. In general, the atomic scattering can be expressed as

$$f(E) = f_0(E) + f'(E) + if''(E), \quad (1)$$

where E is the energy of the probing x rays. The parameters f' and f'' are the real and imaginary parts of anomalous dispersion. They both vary sharply at energies within 10 eV of the absorption edge. The imaginary scattering factor f'' represents the absorption of x rays that results in the photoemission of a core electron.

As has been done in many GISAXS experiments,^{12–15,18,19} the interference between the surface

roughness and the particle scattering is neglected. This assumption is acceptable unless the correlation between the random surface roughness of the substrate and particle position is expected.¹³ Then GISAXS intensity could be written as

$$I(\mathbf{q}) = I_S(\mathbf{q}) + I_p(\mathbf{q}), \quad (2)$$

where \mathbf{q} is the momentum transfer ($|\mathbf{q}| = 4\pi \sin(\theta)/\lambda$, where 2θ is the scattering angle and λ is the wavelength of the x rays). $I_S(\mathbf{q})$ and $I_p(\mathbf{q})$ are the scattering intensities of the surface roughness and the particles. If there was a blank substrate which had the same surface roughness and the same reflective index with those of a substrate used to support a sample, $I_S(\mathbf{q})$ can be obtained and subtracted. Or when the coverage is high enough that $I_p(\mathbf{q})$ is much greater than $I_S(\mathbf{q})$, the background can be neglected. Except for these conditions, background subtraction is not straightforward. For low coverage of a particle, $I_S(\mathbf{q})$ of a substrate for an area ($L_x L_y$) is defined as²⁰

$$I_S(\mathbf{q}) = (n_s f_s)^2 L_x L_y S_S(\mathbf{q}), \quad (3)$$

where

$$S_S(\mathbf{q}) = \frac{2\pi}{q_z^2} \int_0^\infty dR \cdot R \cdot e^{-q_z^2 g(R)/2} J_0(q_{\parallel} R). \quad (4)$$

$S_S(\mathbf{q})$ is defined as the scattering function per unit area surface for an isotropic rough surface and is expressed in terms of q_z and $q_{\parallel} = (q_x^2 + q_y^2)^{1/2}$, which are out-of-plane and in-plane components of \mathbf{q} . The surface roughness is modeled and represented by the distribution function $g(X, Y) \equiv \langle [z(x', y') - z(x, y)]^2 \rangle$, where $z(x, y)$ is the height of the surface above the plane at the coordinates (x, y) , $(X, Y) \equiv (x' - x, y' - y)$, and $R \equiv (X^2 + Y^2)^{1/2}$. n_s and f_s stand for the average atomic number density and average atomic scattering factor of a substrate. Thus, the asymptotic behaviors of $I_S(\mathbf{q})$ should be highly dependent on a model of $g(X, Y)$. When the coverage is high enough, $I_S(\mathbf{q})$ of a substrate surface typically becomes negligible compared to $I_p(\mathbf{q})$ of metal particles. If the homogeneous film is formed on a substrate making an atomic scale interface, correlation between the top surface of the Pt layer and its interface with a substrate should be taken into account.²¹ This limit will not be considered here. When N particles are on the substrate, scattering cross section of the particles is written as

$$I_p(\mathbf{q}, E) = N(n_p f_p(E))^2 S_p(\mathbf{q}), \quad (5)$$

where $S_p(\mathbf{q})$ is a scattering function of a single particle. n_p and f_p are the number density of an atom and atomic scattering factor of a particle. On the other hand, when every N platinum particle is embedded completely in the substrate, the equation is

$$I_p(\mathbf{q}, E) = N(n_p f_p(E) - n_s f_s(E))^2 S_p(\mathbf{q}). \quad (6)$$

In this work, the particle is assumed as composed of a single atomic species.

Since the atomic scattering factors of Si and O are nearly constant in the energy region of the L_3 -absorption edge of Pt which will be designated as E_{Pt} , $I_S(\mathbf{q})$ is almost x-ray energy

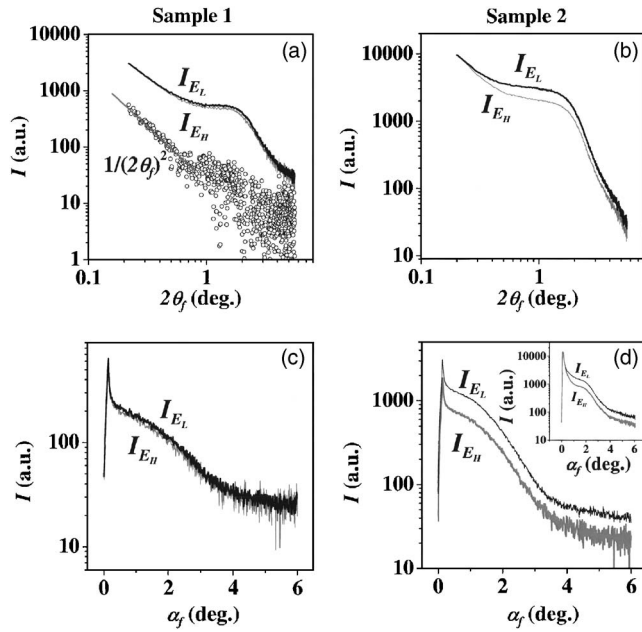


FIG. 2. The fluorescence-subtracted horizontal cuts at $\alpha_f=0.14^\circ$ for samples 1 and 2 are plotted in (a) and (b), respectively. The fluorescence-subtracted vertical cuts at $2\theta_f=1^\circ$ for samples 1 and 2 are plotted in (c) and (d). The circles in (a) represents the particle-scattering subtracted horizontal cut. The inset in (d) corresponds to the vertical cut at $2\theta_f=0.217^\circ$.

independent while $I_p(\mathbf{q}, E)$ is not in this energy region. Simple subtraction of two SAXS curves measured at two different energies, which will be designated as E_L and E_H close to E_{Pt} , yields the almost pure (Pt) metal-particle scattering; when particles are on the substrate,

$$I(\mathbf{q}, E_L) - I(\mathbf{q}, E_H) \equiv I_d(\mathbf{q}) = Nn_p^2 [f_p^2(E_L) - f_p^2(E_H)] S_p(\mathbf{q}). \quad (7)$$

And when particles are embedded in the substrate, it becomes⁸

$$I_d(\mathbf{q}) = Nn_p^2 [f_p^2(E_L) - f_p^2(E_H)] \times \left(1 - \frac{2n_s f_s}{n_p [f_p(E_L) + f_p(E_H)]^2} \right) S_p(\mathbf{q}) \quad (8)$$

(in the case of negligible f'' correction terms), which reduces to

$$I_d(\mathbf{q}) = Nn_p^2 [f_p^2(E_L) - f_p^2(E_H)] S_p(\mathbf{q}), \quad (9)$$

if $2n_s f_s / \{n_p [f_p(E_L) + f_p(E_H)]\} \ll 1$. Simply subtracting the intensities $I_d(\mathbf{q})$ in both equations could be simplified to

$$I_d(\mathbf{q}) \approx Nn_p^2 [2f_{0,p} + f'_p(E_L) + f'_p(E_H)] [f'_p(E_L) - f'_p(E_H)] S_p(\mathbf{q}) = k S_p(\mathbf{q}), \quad (10)$$

where $f_{0,p}$, f'_p , and f''_p are $f_{0,Pt}$, f'_{Pt} and f''_{Pt} , respectively, in this experiment, which are three terms of atomic scattering factor of Pt, and k is an arbitrary scaling factor. In this analysis, we choose 11.342 and 11.552 keV as E_L and E_H , respectively. Variation in f' is responsible for the change in contrast seen in the ASAXS signals.

Figure 2 shows one-dimensional (1D) profiles measured at two different energies of 11.342 (E_L) and 11.552 keV

(E_H). Even though it is difficult to see in the images in Fig. 1, the surface roughness scattering, which is energy independent, is easily determined from the horizontal cut at an exit angle of $\alpha_f=0.14^\circ$ exhibiting a power-law slope of about -2 in this experiment, as shown in Fig. 2(a). For sample 1, the particle scattering occurred as a broad vertical rod, which corresponds to the interparticle distance on a substrate surface and the value is shown in Table I. Its maximum is at about $2\theta_f=1.7^\circ$ and displays small energy dependence in the horizontal cut. For sample 2, the vertical rod moves to a smaller angle and overlaps with the scattering from the surface roughness, since its intensity is higher than that of sample 1 for the higher concentrations of particles. The method used to subtract the fluorescence is explained in the next section. The vertical cuts at $2\theta_f=0.217^\circ$ plotted in the inset of Fig. 2(d) show a clear difference near the critical angle of $\alpha_f=0.14^\circ$, which means that scatterings at $\alpha_f=0.14^\circ$ are energy independent and are from the surface roughness. As expected from Eqs. (7) and (9), anomalous effects become stronger as the number of Pt atoms on the substrate is increased. For sample 4, $I_d(\mathbf{q})$ was overlapped with measured $I(\mathbf{q}, E_L)$ in a log scale, indicating that $I_s(\mathbf{q})$ is negligible, which is not shown here.

Since the effect of f'' occurs as fluorescence, which is approximately q independent in SAXS region, it is inevitably measured near the absorption edge. The magnitude of this effect was calculated and subtracted in Fig. 2 based on the following: because the surface roughness scattering is negligible at high angle, such as $2\theta_f=1^\circ$ near peak maxima, all vertical cuts are fitted with the following equation and the fractions of fluorescence are determined.

$$I_{E_m} = m I_{E_L} + F, \quad (11)$$

where I_{E_L} and I_{E_m} stand for the scattering intensity at energies of $E_L=11.342$ keV and $E_m=11.422-11.568$ keV, respectively, F for the fluorescence and m for the factor corresponding to $(f_{E_m}/f_{E_L})^2$. At the energy E_L , no fluorescence was assumed. Figure 3 shows that the m values [Fig. 3(a)] and fitted fluorescence [Fig. 3(b)] have maxima and minima at the edge, respectively.

The extracted signal is then fitted by using the polydispersed cylinder model with an assumption of coupling height with radius, local monodispersed approximation for coupling of the particle nature and position,²⁴ and distorted wave Born approximation for the reflection and refraction effects of an x-ray beam.^{12,14,15,19} The GISAXS intensities are fitted with the following equation:

$$S_p(\mathbf{q}) = \overline{n(r_0, \sigma) |F(\mathbf{q})|^2} S(\mathbf{q}),$$

$$F(q_{\parallel}, k_z^i, k_z^f) = F(q_{\parallel}, k_z^f - k_z^i) + R(\alpha_f) F(q_{\parallel}, -k_z^f - k_z^i) + R(\alpha_i) F(q_{\parallel}, k_z^f + k_z^i) + R(\alpha_i) R(\alpha_f) \times F(q_{\parallel}, k_z^f - k_z^i), \quad (12)$$

and

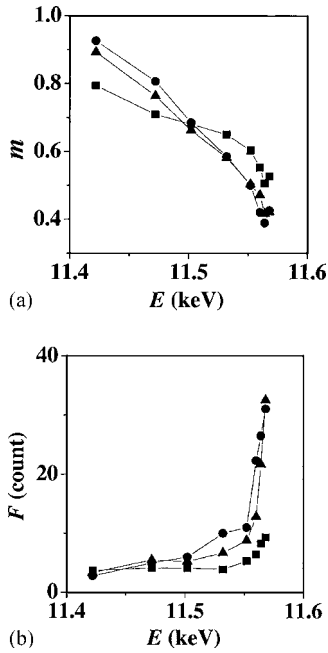


FIG. 3. The m value (a) and the fluorescence intensity (b) for samples 1 (square), 2 (circle), and 3 (triangle) are plotted as a function of x-ray photon energy.

$$n(r_0, \sigma) = \frac{1}{\sqrt{2\pi}r_0\sigma e^{0.5\sigma^2}} e^{-\ln(r/r_0)^2/2\sigma^2}, \quad (13)$$

where $S(\mathbf{q})$ and $F(\mathbf{q})$ are a structure factor and a form factor of a particle, respectively. The Fresnel reflection coefficient on the surface of $\text{SiO}_2/\text{Si}(111)$ wafer calculated by the paratt formalism is R . Here k_z indicates an out-of-plane component of wave vector \mathbf{k} and its superscripts i and f are for the incoming and outgoing directions. The in-plane component of the scattering vector is q_{\parallel} . In the equation, the out-of-plane component q_z is shown as $\pm(k_z^f \pm k_z^i)$. The log-normal size distribution function, $n(r_0, \sigma)$, is assumed with two parameters: r_0 for radius at a maximum population and σ for its broadness. As a model of a particle, a sphere and an oriented cylinder were used in this work. The form factor of a sphere is defined as²²

$$F(q, r) = 4\pi r^3 \frac{\sin(qr) - qr \cos(qr)}{(qr)^3}, \quad (14)$$

where r is a radius of a particle. Average radii of gyration are calculated based on fit parameters according to the definition²²

$$\langle R_g^2 \rangle = \frac{\sum R_g(r)^2 n(r) \nu(r)^2}{\sum n(r) \nu(r)^2}, \quad (15)$$

where ν is the volume of a particles. Corresponding average radii of gyration, which will be designated as R_g instead of $\sqrt{\langle R_g^2 \rangle}$, for a sphere is

$$R_{g,X} = \sqrt{\frac{\sum 3/5 \cdot r^2 n(r) (4\pi r^3/3)^2}{\sum n(r) (4\pi r^3/3)^2}}, \quad (16)$$

where X is o and i for out of plane and in plane, respectively.

The form factor equation of an oriented cylinder is¹⁴

$$F(\mathbf{q}, r, h) = 2\pi r^2 h \frac{J_1(q_{\parallel} r)}{q_{\parallel} r} \frac{2 \sin(q_z h)}{q_z h} \exp(-iq_z h/2), \quad (17)$$

where h is the height of a cylinder. Radii of gyration along the in-plane direction are calculated with a similar fashion as defined in Eq. (15) and derived as

$$R_{g,i} = \sqrt{\frac{\sum 1/2 \cdot r^2 n(r) (\pi r^2 h)^2}{\sum n(r) (\pi r^2 h)^2}}. \quad (18)$$

For the structure factor $S(\mathbf{q})$, we used the 2D paracrystal model [Eq. (19)]¹⁴ and hard-sphere potential model [Eq. (20)]²⁶ which are

$$S(q) = \frac{1 - e^{-2q^2 \sigma_p^2}}{1 - 2e^{-q^2 \sigma_p^2} \cos(q\bar{d}) + e^{-2q^2 \sigma_p^2}} \quad (19)$$

and

$$S(q) = 1/[1 + 24\eta G(2R_{\text{HS}}q)/(2R_{\text{HS}}q)], \quad (20a)$$

respectively, where σ_p and \bar{d} stand for the Gaussian width of the distance distribution of positions of particles and the average distance. η and R_{HS} are for the volume fraction of the particles and their average hard-sphere radius which corresponds to $\bar{d}/2$. The G function in Eq. (20a) is defined as

$$G(A) = \alpha(\sin A - A \cos A)/A^2 + \beta[2A \sin A + (2 - A^2)\cos A - 2]/A^3 + \gamma[-A \cos A + 4((3A^2 - 6)\cos A + (A^3 - 6A)\sin A + 6)]/A^5,$$

$$\alpha = (1 + 2\eta)^2/(1 - \eta)^4, \quad (20b)$$

$$\beta = -6\eta(1 + \eta/2)^2/(1 - \eta)^4,$$

$$\gamma = \eta\alpha/2.$$

Because clusters are deposited one by one on a surface where the potential is isotropic along in-plane direction not along the out-of-plane direction, physically the 2D paracrystal model¹⁴ seems more appropriate rather than those structure factors which assume certain isotropic potentials and equilibrium states. The hard-sphere potential model is used in this paper, because it gives slightly better fits.

Figure 4 shows the simulated 2D data and best fits of horizontal and vertical cuts to a polydispersed cylinder and sphere models. It is noticeable in a GISAXS image of sample 1 in Fig. 2 that the structure factor, which shows up as a broad vertical rod, occurs in in-plane direction only, which means particles are sitting on the substrate like an island and not stacked on each other. Thus, structure factor $S(\mathbf{q})$ is replaced with $S(q_{\parallel})$ in data fitting. Interparticle distance D in Table I is calculated from the maximum position in the fitted structure factor not from that in the raw data. A sphere and an oriented cylinder were tested as representative models of isotropic and anisotropic shapes, respectively. As shown in Eqs. (14) and (17), scattering intensity of a sphere is a function of $|\mathbf{q}| = \sqrt{q_{\parallel}^2 + q_z^2}$, while that of an oriented cylinder is a function

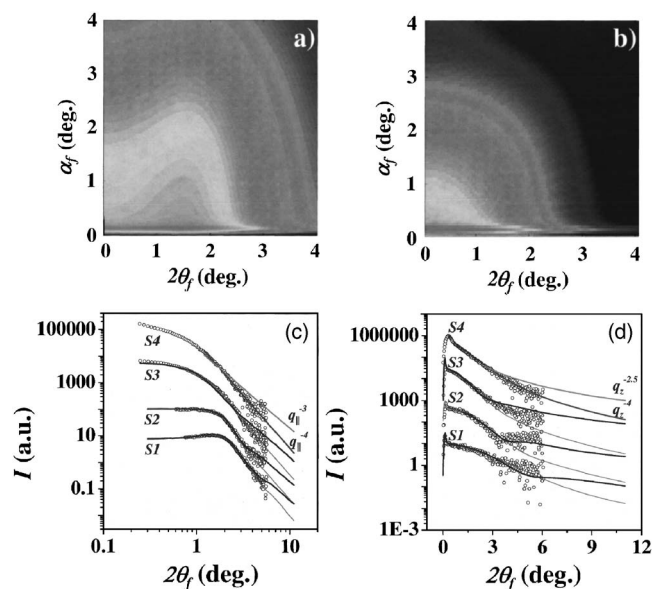


FIG. 4. Plots (a) and (b) show the simulated two-dimensional GISAXS images of Pt nanoparticles in logarithmic scales for samples 1 and 2, which are calculated based on the results of simultaneous data fits of the horizontal (c) and vertical (d) cuts to a polydispersed cylinder model. Fits of a polydispersed cylinder (thick lines) and sphere (thin lines) models are plotted with arbitrarily scaled horizontal cuts at $\alpha_f = 0.154^\circ$ (c) and vertical cuts at $2\theta_f = 1^\circ$ (d) for sample 1 (S1), 2 (S2), 3 (S3), and 4 (S4).

of q_{\parallel} and q_z independently. Since sizes of particles along in plane and out of plane are different as shown in Table I, simultaneous fitting of horizontal and vertical cuts with a sphere model was not possible. In this case, those of both directions are fitted independently. However, when using a polydisperse cylinder model, both directions could be fitted simultaneously using this anisotropic model. Thus background free scattering intensities of Pt particles (without surface roughness scatterings) could be simulated in 2D, as shown in Figs. 4(a) and 4(b). Best fits of a polydisperse cylinder and sphere models are compared in Figs. 4(c) and 4(d). Since scatterings in the Guinier region are only size dependent and not shape dependent, intensities at the small-angle regions are independent of models regardless of whether the in-plane or the out-of-plane slices are taken, whereas asymptotic behaviors at high angle regions are not. In general, at sufficiently high angles, intensity varies as q^{-n} with an exponent n that depends on the sharpness of the island.¹³ It is known that, at $q_{\parallel}R$ or $q_zH > 3.5$, $n=3$ for a cylinder in the in-plane direction and 2.5 in the out-of-plane direction. It is 4 and 3 for a hemisphere in both directions, respectively, and 4 for a sphere regardless of direction.¹³ Asymptotic behaviors of samples 1 and 2 are considerably closer to those of a cylinder than a sphere relatively. The exponent of sample 4 is almost 4 which is a characteristic exponent of a sphere shape. If this is taken into account, that of sample 3, which is neither that of a cylinder or a sphere, seems on the transition from a cylinder (anisotropic) to a sphere (isotropic) shape. This trend is also found in the size differences of particles in the in plane and out of direction, which is discussed below.

Table I shows the summary of the fitting and Guinier analysis results. Since the reflection and refraction are occur-

ring along the out-of-plane direction [vertical cuts, Eq. (12)], the kinematic approach such as Guinier analysis can be applied to the horizontal cuts. Unless the size of the particle is large enough (about tens of nanometers), so that the Guinier region of the scattering from the particle occurs below $\alpha_f = \alpha_{c,s}$, Guinier analysis can be applied to the vertical cuts too. Though they are now shown here, radii of gyration by Guinier analysis were the same as those calculated from a fitted distribution functions regardless of models, a cylinder or a sphere, within 1–2-Å differences. With increasing levels of surface coverage (increased number of laser shots), the size of the particles increases and becomes more polydispersed. Interparticle distances (D) become longer rather than shorter even though the amount of deposited clusters is increased, which also indicates that the islands formed by the cluster agglomeration become larger. Interestingly, together with asymptotic behaviors of GISAXS profiles which tell about the changes of Pt particle shapes as described above, the relative differences in sizes of Pt particles along the in-plane and out-of-plane directions, which is a size anisotropy, were reduced as the coverage of a cluster increased. Although the anisotropy is not so huge, it is obviously distinctive.

This AGISAXS result is understood as the following: A single Pt cluster which is composed of a small number of Pt atoms probably has an anisotropic shape or a facet. The clusters are agglomerated to a nanoparticle whose size gets larger as the amount of the deposited clusters is increased. When the size of the nanoparticle is small and composed of a single or low number of clusters, the nanoparticle might still maintain the shape of a cluster which probably is far from a sphere but close to a cylinder or a hemisphere. As more clusters are agglomerated, being randomly oriented on a surface of nanoparticle, nanoparticles will be larger in size and isotropic in shape.

These changes of Pt nanoparticles might appear in a different way when they are prepared on a different substrate. Several studies on Pt particles grown on different substrates have been published and clearly demonstrated the effect of the substrate on nanoparticle growth.^{27,28} In the case of the $\gamma\text{-Al}_2\text{O}_3(111)/\text{NiAl}(110)$ substrate, which strongly interacts with a Pt cluster, islands grow epitaxially and their height/radius ratio does not change.²⁷ On the contrary, on an amorphous SiO_2 , of which the surface energy is about 1.5 J/m^2 and is roughly 50% of that of Pt,²⁹ the nanoparticles grow randomly.²⁸ Our results interestingly tell that Pt islands grown from clusters on $\text{SiO}_2/\text{Si}(111)$, of which the surface is amorphous, has an anisotropic shape rather than an isotropic form if their sizes are smaller than 1–2 nm.

IV. CONCLUSIONS

In summary, we have demonstrated that AGISAXS is a powerful method to analyze and interpret GISAXS patterns containing mixed scattering from surface roughness and from supported particles. Particle scattering is well separated from that of surface roughness, as well as from particle fluorescence. The background free particle scattering intensities obtained by the anomalous technique are then fitted to mod-

els of polydisperse cylinder and sphere models with DWBA based theory. The results indicate that the sizes of Pt nanoparticles formed on the SiO₂/Si(111) became larger with increasing levels of surface coverage of deposited clusters and the shapes of the supported particles changed from anisotropic to isotropic, indicating that clusters are agglomerated on an amorphous substrate.

The AGISAXS techniques allowed the determination of the particle size and shapes down to the subnanometer scale regardless of the structure of the substrate surface. Since AGISAXS extracts the particle scattering signal from the total, it can be applied to the study of embedded particles in a film or substrate too. It does not destroy the sample and requires just a short exposure time if done at a high flux synchrotron radiation facility. This technique will be very helpful to *in situ* experiments where the structure of a substrate or a matrix might be expected to change during *in situ* experiments.

ACKNOWLEDGMENTS

The authors express thanks for the use of the APS and work at the Argonne National Laboratory, which was supported by the U.S. Department of Energy, Office of Basic Energy Sciences, Division of Chemical Sciences, Geosciences, and Biosciences under Contract No. W-31-109-ENG-38. They also thank Don Graczyk and co-workers for performing the weight analysis of platinum deposits.

¹F. X. Redl, K.-S. Cho, C. B. Murray, and S. O'Brien, *Nature* (London) **423**, 968 (2003).

²Y. Ohko, T. Tatsuma, T. Fujii, K. Naoi, C. Niwa, Y. Kubota, and A. Fujishima, *Nat. Mater.* **2**, 29 (2003).

³L. D. Socaciu, J. Hagen, J. L. Roux, D. Popolan, T. M. Bernhardt, L. Wöste, and S. Vajda, *J. Chem. Phys.* **120**, 2078 (2004).

⁴W. T. Wallace and R. L. Whetten, *J. Am. Chem. Soc.* **124**, 7499 (2002).

⁵A. Sanchez, S. Abbet, U. Heiz, W.-D. Schneider, H. Hakkinen, R. N. Barnett, and U. Landman, *J. Phys. Chem. A* **103**, 9573 (1999).

⁶M. Haruta and M. Daté, *Appl. Catal., A* **222**, 427 (2001).

⁷M. Valden, S. Pak, X. Lai, and D. W. Goodman, *Catal. Lett.* **56**, 7 (1998).

⁸T. Vad, H.-G. Haubold, N. Waldofner, and H. Bonnemann, *J. Appl. Crystallogr.* **35**, 459 (2002).

⁹H.-G. Haubold, R. Gebhardt, G. Buth, and G. Goerigk, in *Resonant Anomalous X-Ray Scattering*, edited by G. Materlik, C. J. Sparks, and K. Fischer (Elsevier Science, Oxford, 1994), pp. 295–304.

¹⁰S. Seifert, R. E. Winans, D. M. Tiede, and P. Thiyagarajan, *J. Appl. Crystallogr.* **33**, 782 (2000).

¹¹R. E. Winans, S. Vajda, B. Lee, S. J. Riley, S. Seifert, G. Y. Tikhonov, and N. A. Tomczyk, *J. Phys. Chem. B* **108**, 18105 (2004).

¹²G. Renaud, R. Lazzari, C. Revenant *et al.*, *Science* **300**, 1416 (2003).

¹³C. Revenant, F. Leroy, R. Lazzari, G. Renaud, and C. R. Henry, *Phys. Rev. B* **69**, 035411 (2004).

¹⁴R. Lazzari, *J. Appl. Crystallogr.* **35**, 406 (2002).

¹⁵M. Rauscher, T. Salditt, and H. Spohn, *Phys. Rev. B* **52**, 16855 (1995).

¹⁶U. V. Desnica, P. Dubcek, I. D. Desnica-Frankovic, M. Bujan, K. Salamon, O. Milat, S. Bernstorff, and C. W. White, *Nucl. Instrum. Methods Phys. Res. B* **200**, 191 (2003).

¹⁷D. Babonneau, A. Naudon, T. Cabioch, and O. Lyon, *J. Appl. Crystallogr.* **33**, 437 (2000).

¹⁸B. Lee, Y.-H. Park, Y.-T. Hwang, W. Oh, J. Yoon, and M. Ree, *Nat. Mater.* **4**, 147 (2005).

¹⁹B. Lee, I. Park, S. Park, J. Yoon, J. Kim, K.-W. Kim, T. Chang, and M. Ree, *Macromolecules* **38**, 4311 (2005).

²⁰S. K. Sinha, E. B. Sirota, S. Garoff, and H. B. Stanley, *Phys. Rev. B* **38**, 2297 (1988).

²¹V. Holy, U. Pietsch, and T. Baumbach, *High-Resolution X-Ray Scattering from Thin Films and Multilayers* (Springer, Berlin, 1999).

²²R.-J. Roe, *Methods of X-ray and Neutron Scattering in Polymer Science* (Oxford University Press, New York, 2000), pp. 155.

²³S. C. Richtsmeier, E. K. Parks, K. Liu, L. G. Pobo, and S. J. Riley, *J. Chem. Phys.* **82**, 3659 (1985).

²⁴E. K. Parks, B. H. Weiller, P. S. Bechthold, W. F. Hoffman, G. C. Nieman, L. G. Pobo, and S. J. Riley, *J. Chem. Phys.* **88**, 1622 (1988).

²⁵Under given experimental conditions, Pt clusters containing up to ~200 atoms were detected on a time-of flight mass spectrometer. S. J. Riley (unpublished).

²⁶J. S. Pedersen, *J. Appl. Crystallogr.* **27**, 595 (1994).

²⁷M. Klimenkov, H. Kühlenbeck, and S. A. Nepijko, *Surf. Sci.* **539**, 31 (2003).

²⁸M. A. Phillips, V. Ramaswamy, B. M. Clemens, and W. D. Nix, *J. Mater. Res.* **15**, 2540 (2000).

²⁹Q. Jiang, H. M. Lu, and M. Zhao, *J. Phys.: Condens. Matter* **16**, 521 (2004).